Applied Catalysis B: Environmental 206 (2017) 104–114

Contents lists available at ScienceDirect

Applied Catalysis B: Environmental

journal homepage: www.elsevier.com/locate/apcatb

# Oxygen storage in three-way-catalysts is an equilibrium controlled process: Experimental investigation of the redox thermodynamics

J. Rink[a,b], N. Meister[a,b], F. Herbst[a,b], M. Votsmeier[b,*]

[a] Technische Universität Darmstadt, Alarich-Weiss-Straße 8, 64287 Darmstadt, Germany
[b] Umicore AG & Co. KG, Rodenbacher Chaussee 4, 63403 Hanau, Germany

ARTICLE INFO

*Article history:*
Received 27 September 2016
Received in revised form
15 December 2016
Accepted 21 December 2016
Available online 23 December 2016

ABSTRACT

A titration method is presented that measures the redox thermodynamics of oxygen storage in three way catalysts under typical operating conditions. The titration scheme starts with an oxygen pulse to completely oxidize the catalyst. The catalyst is then brought into equilibrium with an $H_2/H_2O$ mixture and the resulting oxidation state is determined from the amount of $H_2$ consumed to establish the equilibrium. Measurements were performed in the temperature range of 300 °C–500 °C for two commercial three-way catalysts containing a doped ceria-zirconia solid solution of the composition $Ce_{0.404}Zr_{0.552}Nd_{0.044}O_{1.978}$. The results confirm that under typical automotive operating conditions the oxygen available from the oxygen storage is limited by the equilibrium thermodynamics. Even under very rich conditions (8000 ppm $H_2$/10% $H_2O$) at 500 °C only about 20% of the theoretically available oxygen can be used. At the typical steady state operating point of a three-way catalyst (lambda sensor voltage of 650 mV, 70 ppm $H_2$), at 500 °C only about 6% of the ceria is reduced. Virtually identical oxygen storage performance is obtained for two catalysts with identical oxide composition but different precious metal loadings of 100 g/ft$^3$ and 10 g/ft$^3$.

In a second part of the study, the dynamical oxygen breakthrough is studied experimentally in the $H_2/H_2O/O_2$ system. First, the catalyst is brought into the typical steady state oxidation state and then it is exposed to an oxygen pulse of varying length.

If the thermodynamic data is implemented in a kinetic model, the $H_2$ and $O_2$ signals during the dynamic oxygen breakthrough experiments are very well described. A sensitivity study shows that the $H_2$ response to small $O_2$ pulses, where no $O_2$ breakthrough is observed yet, is completely controlled by the thermodynamics of the oxygen storage. As the $O_2$ pulses get longer and $O_2$ breakthrough is observed, besides thermodynamics also kinetics and internal as well as external mass transfer become important.

© 2017 Elsevier B.V. All rights reserved.

## 1. Introduction

Ceria based materials play an important role as oxygen storage components in three-way catalysts. Due to their ability to store and release oxygen, these materials can buffer fluctuations in the exhaust stoichiometry so that the stoichiometry stays in the small window required for simultaneous conversion of the three pollutants NO, CO and hydrocarbons.

In case of a momentary fuel excess, the ceria buffer can react with reducing exhaust components and releases oxygen, for example by the following reactions:

$$CeO_2 + \frac{1}{2}H_2 \rightleftharpoons CeO_{1.5} + \frac{1}{2}H_2O \quad \text{(R1)}$$

$$CeO_2 + \frac{1}{2}CO \rightleftharpoons CeO_{1.5} + \frac{1}{2}CO_2 \quad \text{(R2)}$$

During a momentary oxygen excess, reduced ceria is oxidized and removes oxygen from the exhaust:

$$CeO_2 \rightleftharpoons CeO_{1.5} + \frac{1}{4}O_2 \quad \text{(R3)}$$

Among the many transition metal oxides that can undergo a change in their oxidation state, ceria and its mixed oxides are the oxygen storage materials of choice for automotive applications. Due to the formation of a nonstoichiometric phase $CeO_x$, these materials

* Corresponding author.
*E-mail address:* martin.votsmeier@eu.umicore.com (M. Votsmeier).

http://dx.doi.org/10.1016/j.apcatb.2016.12.052
0926-3373/© 2017 Elsevier B.V. All rights reserved.

can release a large amount of oxygen while the Ce lattice stays intact so that after reoxidation the original structure is recovered. Today, pure ceria has been replaced by Ce/Zr mixed oxides due to their better thermal stability and greater ability to release oxygen [1–3].

This paper focusses on the thermodynamics of the oxygen storage process. In the automotive application, the redox thermodynamics of the Ce/Zr-oxides are of great relevance since the exhaust always contains $H_2O$ and $CO_2$ which can oxidize the reduced ceria according to the reverse reactions of (R1) and (R2). Previous work suggests that these backward reactions play an important role and that the dynamic response of the catalytic converter is to a large extend determined by the equilibria of reactions (R1) and (R2) [4]. To describe these equilibria, thermodynamic data for the reduction of Ce/Zr mixed oxides is required.

The standard way to describe the redox thermodynamics of metal oxides is to report the oxygen equilibrium pressure for the decomposition reaction of the oxides, in this case (R3). One should be aware, that in this context the term 'equilibrium pressure' is used as a convenient way to describe the oxygen chemical potential or fugacity of the oxide. In most cases, the values of the nominal equilibrium pressure are so low, that in equilibrium not a single oxygen molecule would be found in the reactor, and the equilibrium is clearly not established by molecular $O_2$. Due to the formation of a nonstoichiometric phase, the oxygen equilibrium pressure of ceria and its mixed oxides depends on the degree of reduction (the x in $CeO_x$). If the equilibrium pressure is known, the equilibria for other reactions like (R1) and (R2) can be computed using tabulated gas phase thermodynamic data. While the thermodynamics of pure ceria is well investigated [5–9], surprisingly little work has been done on the thermodynamics of Ce/Zr oxides.

First measurements of the equilibrium oxygen pressure of a Ce/Zr mixed oxide have been performed by Otobe et al. [10], who studied the pyrochlore ($Ce_2Zr_2O_7$/κ-$Ce_2Zr_2O_8$) system, a 1/1 mixed oxide of Ce and Zr with an ordered arrangement of the Ce- and Zr-cations. First data on solid solutions with different Ce/Zr ratios were reported in a series of papers by Gorte and coworkers [11–13]. They found that surprisingly the enthalpies of reduction do not change much with the Ce/Zr ratio or with the degree of reduction and are very similar to the reduction enthalpy of the ordered κ-$Ce_2Zr_2O_8$ phase. This finding was explained by the assumption that also the unordered solid solutions contain pyrochlore-like local entities and that oxygen is mainly released from these entities [12]. The fact that the energy required for the oxygen release is determined by the local environment and local relaxation effects has later been confirmed by DFT calculations [14]. Gorte and coworkers also showed that the equilibrium oxygen pressure does not depend on the crystal size or the precious metal loading of the mixed oxides [12,13]. This suggests that also for nano-scaled high surface area oxides the oxygen release is a bulk phenomenon with little contribution of surface effects. More recently, the redox thermodynamics of Ce/Zr mixed oxides have been investigated in the context of thermal solar water splitting [15,16]. The results of these recent studies are not in good agreement with the earlier work by Gorte et al. All the thermodynamic data on the oxygen release from Ce/Zr mixed oxides described above has been obtained at temperatures of 600 °C and higher and to our knowledge, no data has been reported at the lower temperatures relevant for applications in automotive exhaust catalysis.

For a long time, equilibrium aspects have been largely ignored in the discussion of oxygen storage in three way catalysts. This is particularly obvious if one looks at the way the oxygen storage capacity is defined, how oxygen storage is measured and how it is represented in kinetic models of the three way catalyst.

Oxygen storage capacity conventionally has been measured by subjecting the catalyst to alternating pulses of oxygen and a reductant (mainly $H_2$ or CO) in the absence of $CO_2$ or water [9,17–21]. From a thermodynamic point of view, exposure to CO or $H_2$ in the absence of $H_2O$ and $CO_2$ would lead to complete reduction of the ceria, i.e. to the formation of $CeO_{1.5}$. In reality, complete reduction is not obtained due to kinetic limitations. The fact that measured storage capacities are controlled by kinetic limitations also explains why different values for the storage capacity are obtained by different test protocols. For example, more complete reduction is obtained by long pulses compared to short pulses which led to the distinction between 'fast' and 'slow' OSC (also referred to as 'complete' OSC) [18,21–25]. All the previously published OSC measurements have in common that they measure a kinetically limited oxygen uptake and do not take into account equilibrium effects. In this publication we will present a measurement protocol that determines the available oxygen under thermodynamic constraints. We will show that under equilibrium conditions only a fraction of the theoretically available oxygen can be released and that the dynamic response of the catalyst is to a large extent controlled by this thermodynamically available OSC.

The fact that equilibrium effects have commonly been ignored in the discussion of oxygen storage in three way catalytic converters also is reflected in the kinetic models for these catalysts [26]. Typical literature models took into account the reduction of ceria by CO (via (R2)), $H_2$ (via (R1)) and potentially hydrocarbons. Oxidation was assumed to proceed through the oxidation by $O_2$ (via (R3)) or NO. The oxidation of reduced ceria by $H_2O$ (reverse reaction of (R1)) and by $CO_2$ (reverse reaction of (R2)) generally was neglected, although the exhaust contains about 10% of $H_2O$ and $CO_2$ and it is well known that under relevant operating conditions reduced ceria can be oxidized by these compounds [27–30]. A short literature overview on the modeling of oxygen storage in three way catalysts was provided in [4]. The main shortcoming of kinetic models ignoring equilibrium effects is that these models predict a complete reduction to $CeO_{1.5}$ in the presence of reductants like $H_2$ or CO, while in reality, due to the reoxidation by $H_2O$ and $CO_2$ only a partial reduction can be achieved.

In a previous paper, we introduced a kinetic model for the oxygen storage on ceria that takes into account the reoxidation by $H_2O$ and $CO_2$ and hence includes the equilibrium effects [4]. In this paper, it was shown that a number of experimental observations relevant for the understanding of lambda control can only be explained if equilibrium effects are appropriately considered. These observations include:

- The experimentally measured oxygen storage capacity depends on the amplitude of the lambda pulses.
- Lambda oscillations can be completely buffered by the oxygen storage even if the average lambda is slightly rich.
- The shape of the breakthrough curve after rich-lean step.
- The delayed CO and $H_2$ emissions after the completely oxidized catalyst has been reduced by a rich pulse, the so called fuel cut scenario.
- The fact that during steady state operation the filling level of the oxygen storage can be induced from the lambda signal behind the catalyst. This effect is the basis of the currently employed algorithms using a second lambda probe behind the catalyst.

Although all these effects could be nearly quantitatively described by our simple equilibrium based oxygen storage model, a remaining shortcoming of our previous paper [4] was that the thermodynamic parameters were fit together with kinetic parameters to experimental data. It is in the nature of such a parameter fitting procedure that it is difficult to access, in how far the obtained parameters are uniquely determined by the data and in how far the conclusion of the study is robust to changes in the parameter set.

The approach of the current publication is to provide an independent measurement of the relevant thermodynamic data. To this

end, in a first step a titration method for the measurement of the ceria reduction equilibrium under the conditions relevant in automotive catalysis will be presented. The procedure will be used to characterize the equilibrium properties of the doped ceria-zirconia mixed oxide in a commercial three-way catalyst. In a second step, the dynamic response of the catalyst to short oxygen pulses will be experimentally investigated and it will be analyzed to what extend this response is controlled by the thermodynamics of the oxygen storage.

## 2. Methodology

### 2.1. Experimental

#### 2.1.1. Catalyst samples

Catalysts very similar to a commercial three-way catalyst from Umicore AG & Co. KG were used. A conventional cordierite substrate with square channels and a cell density of 600 cpsi was coated with washcoat consisting of precious metals and a Ce/Zr mixed oxide oxygen storage. Most of the measurements reported in this paper were obtained using a catalyst with the precious metal loading of 10 g/ft$^3$ (5 g/ft$^3$ Rh, 3 g/ft$^3$ Pd and 2 g/ft$^3$ Pt). In section 3.2, some measurements are reported for a catalyst with the higher precious metal loading of 100 g/ft$^3$ (10 g/ft$^3$ Rh, 80 g/ft$^3$ Pd and 10 g/ft$^3$ Pt), which is the same catalyst as used in our previous study [4,31]. Besides the precious metal loading, both catalysts had the same washcoat composition and contained a mixed oxide of the composition $Ce_{0.40}Zr_{0.55}Nd_{0.044}O_{1.978}$ as oxygen storage material. The catalysts were aged in air for 16 h at 985 °C.

#### 2.1.2. Model-gas test bench

All experiments were carried out in a laboratory reactor. The exhaust gas was mixed from bottles and heated to the desired temperature before entering the catalyst. A thermocouple placed directly in front of the catalyst was used to control the inlet temperature. Hydrogen and oxygen were injected via mass flow controllers with a fast response time, while water was supplied by an evaporator. A comparable test bench is described in [32].

The inlet concentrations were recorded using the signals of the mass flow controllers, whereas the outlet concentrations of $H_2$, $O_2$ and $H_2O$ were measured with an Omnistar mass spectrometer from Pfeiffer Vacuum.

### 2.2. Simulation

#### 2.2.1. Mathematical model

All channels within the catalytic converter are assumed to behave identically and a single channel model is used to describe the behavior of the three-way catalytic converter. For the modeled channel, a 1D + 1D model accounting for diffusion within the washcoat is utilized.

In the gas phase, radial gradients of the temperature and concentrations are neglected and the heat/mass balance equations are solved in terms of lumped velocity averaged values:

$$\frac{\partial c_{gas,i}}{\partial t} = -v_{gas}\frac{\partial c_{gas,i}}{\partial z} - \beta_i \frac{4}{D_H}\left(c_{gas,i} - c_{wc,i}\right) \tag{1}$$

$$\frac{\partial T_{gas}}{\partial t} = -v_{gas}\frac{\partial T_{gas}}{\partial z} - \alpha \frac{4}{D_H \cdot \rho_{gas} \cdot c_{p,gas}}\left(T_{gas} - T_s\right) \tag{2}$$

Here, $c_{gas,i}$ is the velocity averaged concentration of species $i$ in the channel and $c_{wc,i}$ is the concentration at the gas-washcoat interface. $T_{gas}$ is the velocity averaged temperature in the gas phase and $T_s$ is the temperature of the solid phase (washcoat + substrate). The average gas velocity is represented by $v_{gas}$, while $t$ is the time coordinate and $z$ the axial position in the reactor. The radial mass and heat transfer between the gas phase and the washcoat is described by heat- and mass transfer coefficients, $\alpha$ and $\beta_i$, respectively. The position dependent transfer coefficients are computed via the correlation presented in [33]. Additionally, $D_H$ is the hydraulic diameter, $\rho_{gas}$ represents the gas phase density and $c_{p,gas}$ is the heat capacity of the gas phase.

In the washcoat, reactions, radial diffusion and mass transfer from the surface to the gas phase take place. The corresponding mass balance is solved for in Eq. (3) with the boundary conditions given by Eq. (4).

$$\frac{\partial c_{wc,i}}{\partial t} = -D_{eff,i}\frac{\partial^2 c_{wc,i}}{\partial r^2} + \sum_j \nu_{i,j} R_j \tag{3}$$

$$D_{eff,i}\frac{\partial c_{wc,i}}{\partial r}\Big|_{x=0} = \beta_i\left(c_{wc,i}|_{x=0} - c_{gas,i}\right) \tag{4}$$

In the equations above, $D_{eff,i}$ is the effective diffusion coefficient of species $i$ in the washcoat, $R_j$ the reaction rate of reaction $j$ and $\nu_{i,j}$ the stoichiometric coefficient of species $i$ in reaction $j$, whereas $r$ represents the radial position in the washcoat.

For the energy balance, the washcoat and the substrate are lumped into one phase, since conduction between these two phases is assumed fast. The temperature of the solid phase $T_s$ is solved for in Eq. (5).

$$\frac{\partial T_s}{\partial t} = \alpha \frac{4}{D_H \cdot \rho_s \cdot c_{p,s}}\left(T_{gas} - T_s\right) + \frac{1}{\rho_s c_{p,s}}\int_0^{d_{wc}} \Delta_R H_j R_j dr \tag{5}$$

In Eq. (5), $\rho_s$ and $c_{p,s}$ are the density and heat capacity of the solid phase, respectively, and $\Delta_R H_j$ represents the reaction enthalpy of reaction $j$.

#### 2.2.2. Kinetic model

The kinetic model is adapted from Moeller et al. and comprises the three reactions ((R1)–(R3)) [4]. For the reaction rates power laws are used (Eqs. (6)–(8)).

$$R_1^f = k_2^f c_{H_2}\Theta; \quad R_1^b = k_1^b c_{H_2O}\left(1-\Theta\right) \tag{6}$$

$$R_2^f = k_1^f c_{CO}\Theta; \quad R_2^b = k_2^b c_{CO_2}\left(1-\Theta\right) \tag{7}$$

$$R_3^f = k_3^f \Theta^2; \quad R_3^b = k_3^b c_{O_2}\left(1-\Theta\right)^2 \tag{8}$$

Here, $R_i^f$ and $R_i^b$ are the forward and backward reaction rates with their corresponding rate constants $k_i^f$ and $k_i^b$, respectively, $c_i$ the gas species in the washcoat and $\Theta$ the oxidation degree of the oxygen storage as defined in Eq. (9).

$$\Theta = \frac{c_{CeO_2}}{c_{CeO_2} + c_{CeO_{1.5}}} \tag{9}$$

In our model implementation, the backward reaction rate constants $k_i^b$ are calculated by the Arrhenius equation (Eq. (10)) with the rate coefficient Ai and the activation energy Eai.

$$k_i^b = A_i e^{-\frac{E_{a,i}}{RT}} \tag{10}$$

The forward reactions rate constants are computed from the chemical equilibrium constant $K_i$ and the backward reaction rate constants (Eq. (11)).

$$k_i^f = k_i^b K_i \tag{11}$$

The equilibrium constant $K_i$ is computed based on the experimental data described in section 3.1. Thermodynamic data of gas phase species was computed from the data base GASEQ [34].

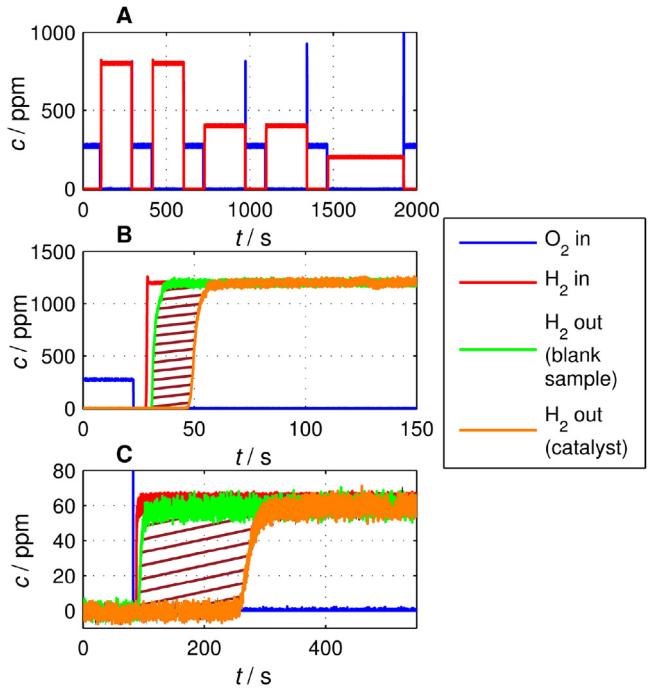


**Fig. 1.** Experimental Setup for the thermodynamic measurements (T = 500 °C, GHSV = 65 000 $h^{-1}$). A) Example of consecutive inlet pulses of oxygen and hydrogen. B) $H_2$ response of catalyst and blank sample for a pulse with 1200 ppm $H_2$. C) $H_2$ response of catalyst and blank sample for a pulse with 60 ppm $H_2$. The experimental OSC is indicated by the hatched area.

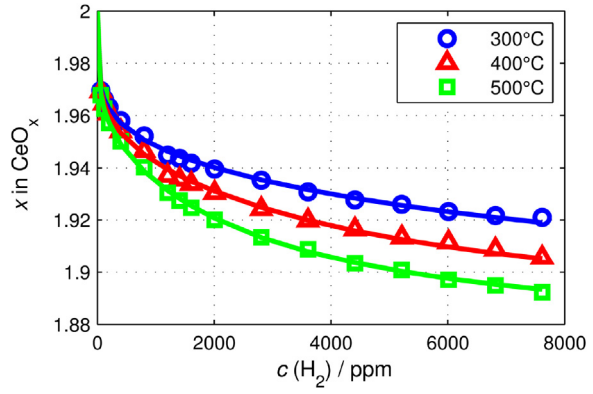


**Fig. 2.** Measured equilibrium composition as a function of the $H_2$ concentration in the gas phase (10% $H_2O$, $N_2$ balance, GHSV = 65 000 $h^{-1}$). In addition to the experimental data (symbols), the polynomial fit used for the computation of the equilibrium constants in the kinetic model is shown (lines).

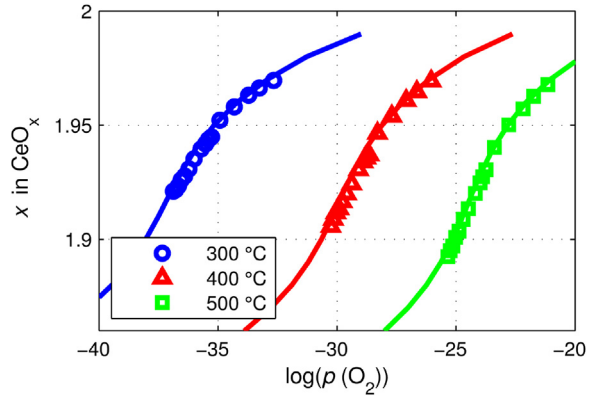


**Fig. 3.** Equilibrium stoichiometry as a function of equilibrium partial pressure. In addition to the experimental data (symbols), the polynomial fit used for the computation of the equilibrium constants in the kinetic model is shown (lines).

## 3. Results and discussion

### 3.1. Measurement of the $Ce/ZrO_2$ redox thermodynamics

The working principle of our thermodynamic measurements is to start with a completely oxidized catalyst, and then to measure the amount of $H_2$ required to bring the oxygen storage into equilibrium with a mixture that contains $H_2/H_2O$. A typical experiment is shown in Fig. 1A. First, an oxygen pulse (300 ppm) is applied to bring the ceria into a completely oxidized state. After a 2 s delay (to avoid direct reaction of $O_2$ and $H_2$), the oxygen pulse is followed by a hydrogen pulse. During the entire pulse sequence, water is dosed in a constant concentration of 10%. At the beginning of the hydrogen pulse, $H_2$ is consumed due to the reaction with $CeO_2$ (reaction (R1)). As it reacts with $H_2$, the ceria gets successively reduced, until reaction (R1) reaches an equilibrium and a breakthrough of $H_2$ is observed. The equilibrium oxidation state of the ceria (the x in $CeO_x$) can be computed from the amount of $H_2$ required to establish the equilibrium. After complete $H_2$ breakthrough is obtained, the hydrogen is switched off and the next measurement cycle is started, again with an initial oxygen pulse. Especially for the higher $H_2$ concentrations, the response time of the $H_2$ measurement becomes comparable to the timescale of the breakthrough experiment. To correct for this effect, the instrument response was measured for each hydrogen concentration with a blank sample. The overall hydrogen take-up was then determined from the area between the breakthrough curves with and without catalyst, see Fig. 1B and C.

The pulse experiments were repeated for a range of hydrogen concentrations and three different temperatures. Fig. 2 summarizes the results of these measurements. It was found that over the full range of conditions, the measured hydrogen uptake is well below the value that would correspond to complete reduction to $CeO_{1.5}$. Even at the highest hydrogen concentration of 0.8% at 500 °C, only 21.3% of the theoretically available oxygen is removed. At the typical steady state operating point of a three way catalyst (near a lambda sensor voltage of 650 mV, 70 ppm $H_2$), at 500 °C only about 6% of the ceria is reduced.

Fig. 3 plots the measured equilibrium stoichiometry as a function of the equilibrium gas phase oxygen pressure $p_{O_2}$. The equilibrium oxygen pressure$p_{O_2}$ of the gas mixture is determined by the equilibrium of the reaction

$$H_2 + \frac{1}{2}O_2 \leftrightharpoons H_2O \qquad \text{(R4)}$$

The equilibrium partial pressure of oxygen $p_{O_2}$ can be computed as:

$$p_{O_2} = \left(\frac{p_{H_2O}}{p_{H_2} \cdot K_W}\right)^2 \qquad (12)$$

where $K_W$ is the equilibrium constant of reaction (R4).

In the literature, thermodynamic results for ceria reduction are generally expressed as the free reaction enthalpy $\Delta_R G(x)$ of the reaction

$$4CeO_{1.5} + O_2 \rightleftharpoons 4CeO_2 \qquad \text{(R5)}$$

With the equilibrium constant for the reaction being defined as

$$K(x) = p_{O_2}^{-1} \qquad (13)$$

the free reaction energy $\Delta_R G(x)$ can then be computed as

$$\Delta_R G(x) = -RT\ln(K(x)) = RT\ln\left(p_{O_2}\right) \qquad (14)$$

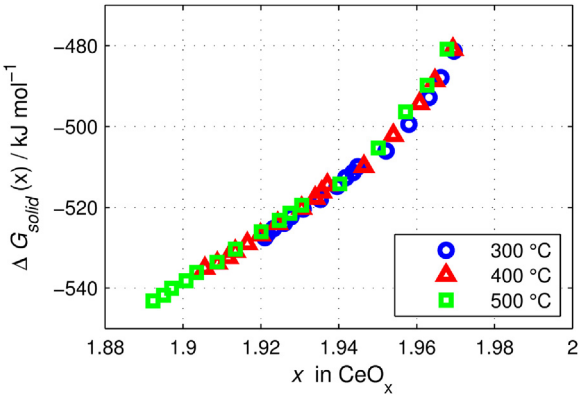


**Fig. 4.** Formation energy of $CeO_x$ as a function of the stoichiometry x.

Note that $\Delta_R G(x)$ is a function of the stoichiometry x of the oxide.

The free reaction energy determined according to Eq. (14) contains contributions from the chemical potentials of the solid phase ($\mu_{CeO_2}(x)$, $\mu_{CeO_{1.5}}(x)$) and from the gas phase ($\mu_{O_2}$):

$$\Delta_R G(x) = 4\mu_{CeO_2}(x) - 4\mu_{CeO_{1.5}}(x) - \mu_{O_2} \quad (15)$$

It is useful to separate solid state from gas phase effects. For this purpose we define a $\Delta G_{solid}(x)$ that only contains the solid state effects. $\Delta G_{solid}(x)$ represents the change in the free energy of the crystal lattice (per uptake of one mole of $O_2$) as $CeO_x$ is oxidized to $CeO_{x+\delta}$:

$$\Delta G_{solid}(x) = 4\mu_{CeO_2}(x) - 4\mu_{CeO_{1.5}}(x) = \Delta_R G(x) + \mu_{O_2} \quad (16)$$

Fig. 4 plots $\Delta G_{solid}(x)$ as a function of x. It can be observed that for a given x, $\Delta G_{solid}(x)$ is nearly temperature independent. This means that entropic contributions to $\Delta G_{solid}(x)$ seem to be small. This is in line with expectations since entropy changes during solid state reactions generally are small compared to enthalpic contributions.

Fig. 4 also shows that $\Delta G_{solid}(x)$ becomes increasingly more negative as the oxide becomes more reduced (x in $CeO_x$ is decreased). This means that with increasing reduction, more and more energy is required to remove an additional oxygen atom. This result is expected, since only when $\Delta G_{solid}(x)$ shows a monotonous increase with x, a nonstoichiometric phase can be formed.

### 3.2. The effect of precious metal loading on the oxygen storage capacity

All measurements reported so far were obtained for a catalyst with a precious metal loading of 10 g/ft$^3$. In our previous study [4], we used a catalyst with a higher precious metal loading of 100 g/ft$^3$ (10 g/ft$^3$ Pt, 80 g/ft$^3$ Pd, 10 g/ft$^3$ Rh). Besides the precious metal loading, both catalysts had the same washcoat composition including an identical ceria mixed oxide of the composition $Ce_{0.40}Zr_{0.55}Nd_{0.044}O_{1.978}$. We performed the thermodynamic titration experiments also for the catalyst with the higher precious metal loading and the results for the two catalysts are compared in Fig. 5. Nearly identical $\Delta_R G$ values were obtained for the two precious metal loadings. Although the higher precious metal loading seems to yield slightly higher (less negative) values for $\Delta_R G(x)$ (which corresponds to slightly higher oxygen storage capacities at a given oxygen partial pressure), the differences are minimal and most likely within the experimental uncertainty. This result is in line with the work of [13] who also found that $\Delta_R G(x)$ is a bulk property of the mixed oxide and is not influenced by the presence of precious metals.

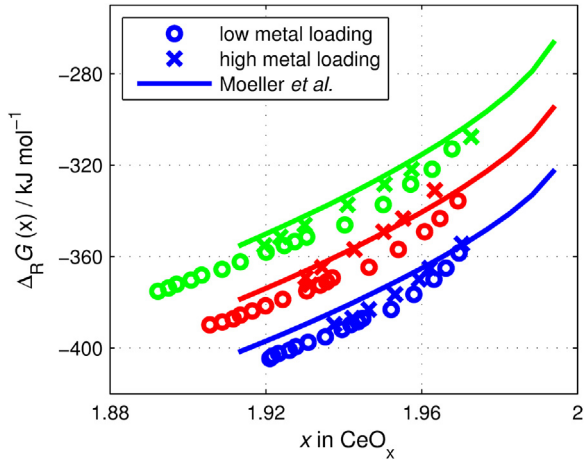


**Fig. 5.** Free Reaction enthalpy of the oxygen storage material as a function of the non-stoichiometry x. The experimental data for the catalyst with a low precious metal loading of 2 g/ft$^3$ Pt, 3 g/ft$^3$ Pd, 5 g/ft$^3$ Rh (circles) is compared to the experimental data for the catalyst with a high precious metal loading of 10 g/ft$^3$ Pt, 80 g/ft$^3$ Pd, 10 g/ft$^3$ Rh (crosses) and the model obtained by Moeller et al. for the highly loaded catalyst by a simultaneous fit of the kinetic and thermodynamic parameters to experimental data [4].

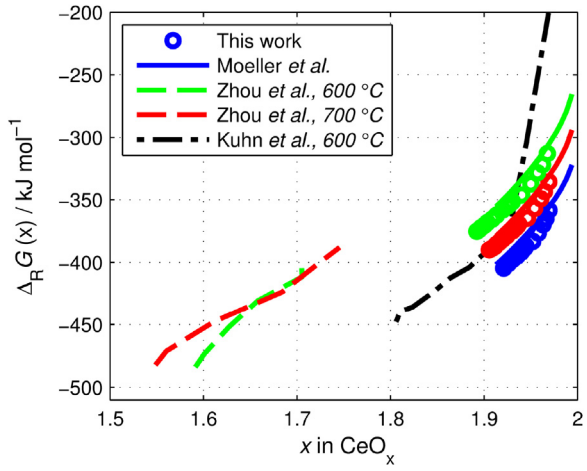


**Fig. 6.** Free Reaction enthalpy of the oxygen storage material as a function of the non-stoichiometry x. The data of this work and from [4] is given for T = 300 °C (blue), T = 400 °C (red) and T = 500 °C (green). The data is compared to the results from [13] and [15]. (For interpretation of the references to colour in this figure legend, the reader is referred to the web version of this article.)

### 3.3. Comparison with literature data

Fig. 5 also compares the results for $\Delta_R G(x)$ obtained in this study to the results of our previous study, where the thermodynamic data was indirectly determined by a simultaneous fit of kinetic and thermodynamic parameters. The previous study used the catalyst with the higher precious metal loading. Fig. 5 shows that the free reaction energy determined indirectly from a fit of the kinetic and thermodynamic parameters to the measured concentration profiles is in surprisingly good agreement with the directly measured data presented in the current publication. Once more, this excellent agreement underlines the high sensitivity of the measured oxygen storage dynamics towards the thermodynamic parameters.

In Fig. 6, our results for the free reaction energy $\Delta_R G(x)$ are compared to literature data. Our results for the temperature range of 300 °C–500 °C extrapolate reasonably well to the results of Zhou et al. obtained at 600 °C for a ceria mixed oxide of a similar composition ($Ce_{0.5}Zr_{0.5}O_2$) [13]. The agreement with the more recent

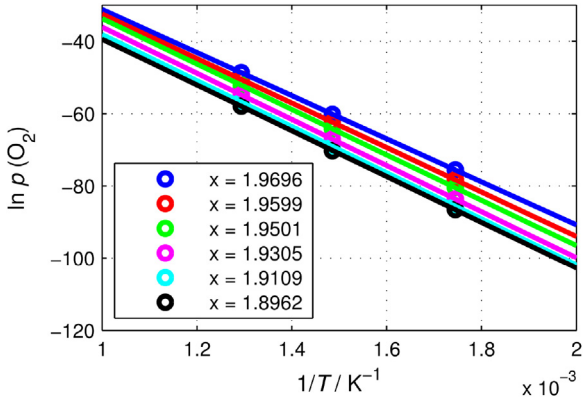


**Fig. 7.** Arrhenius presentation for the oxygen storage material at evaluated non-stoichiometries x.

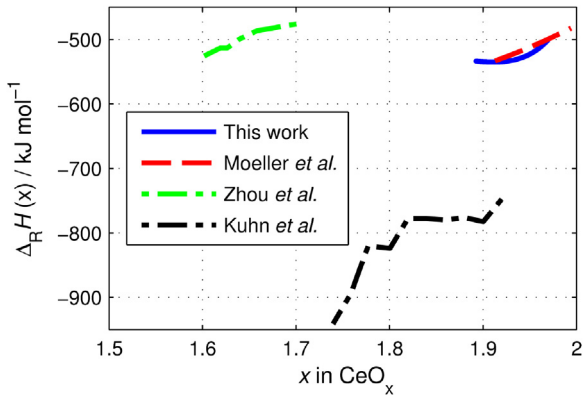


**Fig. 8.** Reaction enthalpy as a function of the non-stoichiometry x for the measured data compared to literature data on $Ce_{0.5}Zr_{0.5}O_2$ [4,13,15].

data obtained by Kuhn et al. for a $Ce_{0.5}Zr_{0.5}O_2$ mixed oxide is less favorable [15].

For different degrees of reduction x, Fig. 7 plots $\ln(p_{O_2})$ as a function of 1/T. For each x, a straight line is obtained which according to Eq. (17) allows the computation of the reaction enthalpies $\Delta_R H(x)$ and the reaction entropies $\Delta_R S(x)$.

$$\ln\left(p_{O_2}\right) = \frac{\Delta_R H(x)}{RT} - \frac{\Delta_R S(x)}{R} \tag{17}$$

As can be seen in Fig. 8, we obtain values for the reaction enthalpy $\Delta_R H(x)$ (note:please use the symbol in the deleted line above) in the range of −520 kJ/mol. This is in very good agreement with the results of our earlier study and with the reaction enthalpies $\Delta_R H(x)$ reported by Zhou et al. for Ce/Zr mixed oxide with a Ce/Zr ratio of 50/50 [13]. The value is also in good agreement with the reaction enthalpy for the oxidation of the ordered $Ce_2Zr_2O_7$ pyrochlore phase as computed by Zhou et al. [13] based on the data of Otobe et al. [10]. Again, less good agreement is found with the recent measurements of Kuhn et al. [15]. However, their value of ∼-850 kJ/mol seems to be high, as it is close to the value of ∼-780 kJ/mol reported for pure ceria [11] and it is generally accepted that the doping with zirconia lowers the oxidation enthalpy [13,16].

Finally, Fig. 9 compares our data for the oxidation entropy to literature data. On the left axis we plot the reaction entropies as reported in the literature. On the right axis we plot a solid phase entropy $\Delta S_{solid}(x)$ defined in analogy to $\Delta G_{solid}(x)$ (Eq. (16)). $\Delta S_{solid}(x)$ represents the change in the crystal lattice's entropy upon removal of an incremental amount of oxygen (per mole of $O_2$). The data reported by Zhou et al. [13] result in a $\Delta S_{solid}(x)$ of

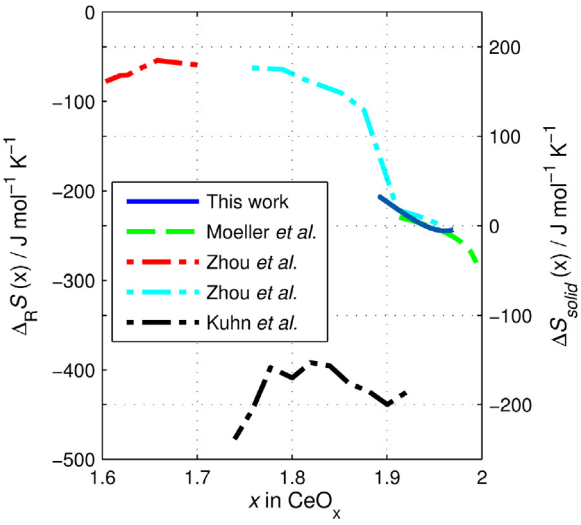


**Fig. 9.** Reaction entropy as a function of the non-stoichiometry x for the measured data compared to literature data [4,13,15]. For [13], two different composition with $Ce_{0.5}Zr_{0.5}O_2$ (red) and $Ce_{0.81}Zr_{0.19}O_2$ (cyan) are shown. The entropy of the solid (right side), is obtained by shifting the data by 239 J/mol K$^{-1}$ ($S(O_2)$ at T = 600 °C). (For interpretation of the references to colour in this figure legend, the reader is referred to the web version of this article.)

200 J/mol/K. This is an unexpectedly high value for a solid state process, since typical reaction entropies for solid state processes are below a few 10 J/mol/K. Similarly, the value of Kuhn et al. (∼−200 J/mol/K) seems to be unrealistically low. Our values are in the range ±30 J/mol/K which is much more consistent with the expected reaction entropies for a solid state process.

### 3.4. The impact of thermodynamics on the dynamic response to $O_2$-pulses

So far, we have discussed the thermodynamics of the oxygen storage. Now, we will – still in the simple $H_2/O_2/H_2O$ system – measure the transient response of the catalyst to a short oxygen pulse. The motivation for these experiments is to investigate in how far the dynamic response of the catalyst can be predicted based on the thermodynamic data and, even more importantly, to which extend the dynamic behavior is controlled by thermodynamics. Oxygen breakthrough after a lean excursion of the exhaust stoichiometry is a scenario of high practical relevance, since in a full exhaust mixture oxygen breakthrough is generally associated with NO breakthrough.

#### 3.4.1. Dynamic response to $O_2$-pulses: experimental results

In the vehicle, the lambda control tries to keep the filling level of the oxygen storage at an intermediate level because in this state the catalyst is equally well prepared for an unforeseen lean or rich lambda excursions. In our experiments this situation is emulated by the following pulse sequence (compare Fig. 10): To bring the oxygen storage into a realistic initial state, the catalyst is continuously subjected to a background mixture of 70 ppm $H_2$ and 10% $H_2O$. Once equilibrium is established, a pulse of 1035 ppm oxygen is injected on top of the $H_2/H_2O$ mixture. The response of the downstream oxygen and $H_2$ concentrations is then monitored, and when an equilibrium is established again, a new oxygen pulse is injected. The full pulse sequence is shown in Figure Fig. 10. In the sequence, the length of the oxygen pulses is successively increased from 2 s to 7 s. Fig. 10B shows the response of the downstream oxygen concentration. The shortest pulses are completely absorbed by the oxygen storage and no breakthrough is detected. At a pulse length of 5 s (pulse no. 4) the oxygen storage can no longer absorb the full pulse

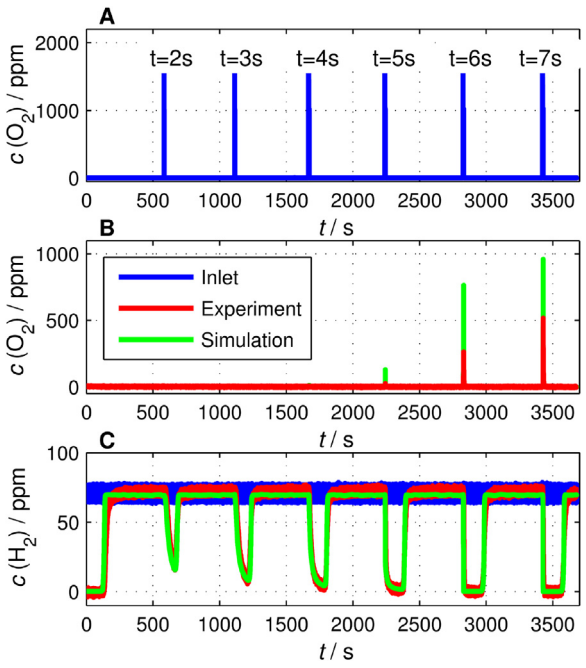


**Fig. 10.** The dynamic response to oxygen pulses of different length (T = 500 °C, GHSV = 65 000 $h^{-1}$): A) The oxygen inlet pulse scheme. B) Experimental and simulated $O_2$ response signal. C) Experimental and simulated $H_2$ response signal.

**Table 1**
Kinetic Parameters used in the simulation model.

| Parameter | Value |
|---|---|
| $A_1$ ($H_2$ reaction) | $7.9 \times 10^{13}$ $s^{-1}$ |
| $E_{a,1}$ ($H_2$ reaction) | 150.9 kJ/mol |
| $A_3$ ($O_2$ reaction) | $5.6 \times 10^4$ $s^{-1}$ |
| $E_{a,3}$ ($O_2$ reaction) | 97.4 kJ/mol |

and an oxygen breakthrough is observed. As the pulse length is further increased, more and more oxygen breaks through. Fig. 10C shows the response of the downstream hydrogen concentration. Even for the shortest pulses, where no oxygen breakthrough occurs, a dip in the hydrogen signal is observed after each oxygen pulse. This response is important for the lambda control since it allows the rear lambda sensor to detect a depletion of oxygen storage before oxygen breaks through.

### 3.4.2. Numerical modeling of the oxygen/hydrogen breakthrough

The interaction of the $O_2/H_2/H_2O$ mixture with the oxygen storage can be described by two reactions ((R1) and (R2)). The two reactions were implemented in a reactor model that describes the flow and mass transport in a single channel of the catalyst. Thermodynamic consistency of the mechanism was ensured by computing the rate of the forward reactions from the equilibrium constants and the backward rates. The equilibrium constant depends on the degree of reduction of the ceria storage (the x in $CeO_x$) and the temperature. It was computed from a polynomial fit of $\Delta_R G(x, T)$ to the data presented in Section 3.1. The fit to the data is shown in Figs. 2 and 3 as a straight line.

Our model as described above contains four kinetic parameters, one preexponential factor and one activation energy for each of the two reactions. For our simulation study, the four kinetic parameters were fit to the amount of oxygen breakthrough as a function of the pulse length and temperature. A typical fit is shown for T = 500 °C in Fig. 11. The kinetic parameters obtained by the fit procedure are provided in Table 1.

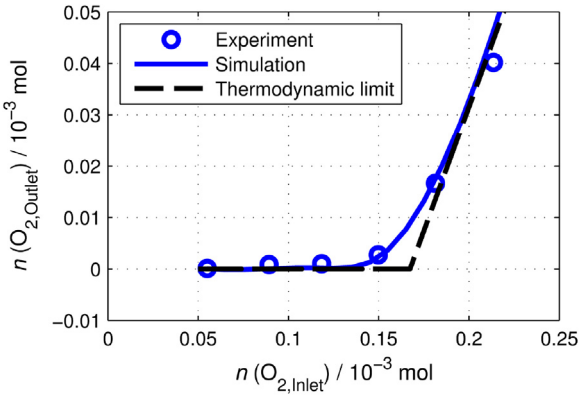


**Fig. 11.** Model parameterization to cumulated oxygen breakthrough (T = 500 °C, GHSV = 65 000 $h^{-1}$). The thermodynamic limit represents the case, in which no limitation due to kinetics or diffusion occurs.

As can be seen in Fig. 10B, the model very well describes the onset of the oxygen breakthrough, while the pulse heights of the breakthrough pulses are not well reproduced. The reason for the misfit in the pulse heights is a broadening of the experimental $O_2$ breakthrough peaks due to the limited time resolution of the $O_2$ analyzer. The time resolution does not affect the integral area below the peak, which is the reason why the integral oxygen breakthrough was chosen as the target of the parameter fitting procedure.

Fig. 11 also shows the oxygen breakthrough that would occur if reactions and transport processes were fast (denoted as the 'Thermodynamic limit'). In this case, breakthrough would only occur after the storage has reached its equilibrium state, i.e. the breakthrough is entirely controlled by the thermodynamically available oxygen storage. In the measurements and the simulations, breakthrough occurs earlier than predicted by the thermodynamic limit, which shows that oxygen breakthrough is also controlled by kinetic and transport limitations.

Although not considered during the parameter fitting procedure, the hydrogen signals are very well reproduced by the model, (compare Fig. 10C). Similar agreement between simulation and experiment is obtained for the experiments at 300 °C and 400 °C, compare FigA 1 and 2 in the accompanying material.

Fig. 12 provides a close up view on the $H_2$ response to the first four pulses. For the first pulse with a duration of 2 s, the $H_2$ signal decreases 10 s after switching of the $O_2$ pulse. The signal decreases slowly until a minimum of 20 ppm is reached, before increasing to 70 ppm again. With an increasing duration of the $O_2$ pulse, the time delay between the end of the pulse and the decrease in the $H_2$ signal becomes shorter and the minimum of the signal decreases. The forth pulse with a duration of 5 s is the first pulse where oxygen breakthrough was observed. Associated with the oxygen breakthrough is an immediate decrease in the $H_2$ signal.

To understand the observed shape of the $H_2$ signal and the underlying processes, it is helpful to compute the development of the concentration profiles along the length of the reactor. Fig. 13 shows the simulated $H_2$ gas phase concentrations in the washcoat and the corresponding filling levels of the oxygen storage for four different time steps after the first oxygen pulse. At the end of the oxygen pulse, the front zone of the catalyst is completely oxidized while in the rear part the oxygen storage is still at the initial filling level. The $H_2$ of the inlet flow is oxidized by the excess oxygen so that the $H_2$ concentration in the front zone of the catalyst is zero. In the rear zone where the oxygen storage is still reduced, $H_2$ is formed by the reaction of $H_2O$ with reduced ceria, so that at the outlet the $H_2$ remains at the initial concentration of 70 ppm. After the oxygen is switched off, the front part of the catalyst is successively reduced by $H_2$ from the feed. At the same time at the rear

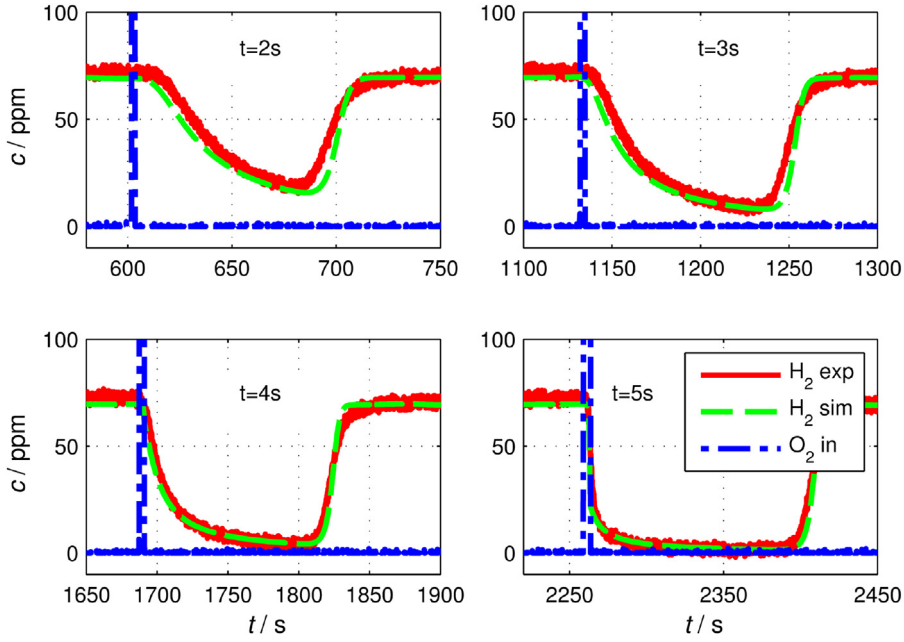


**Fig. 12.** Downstream $H_2$ signal following oxygen pulses with different lengths.

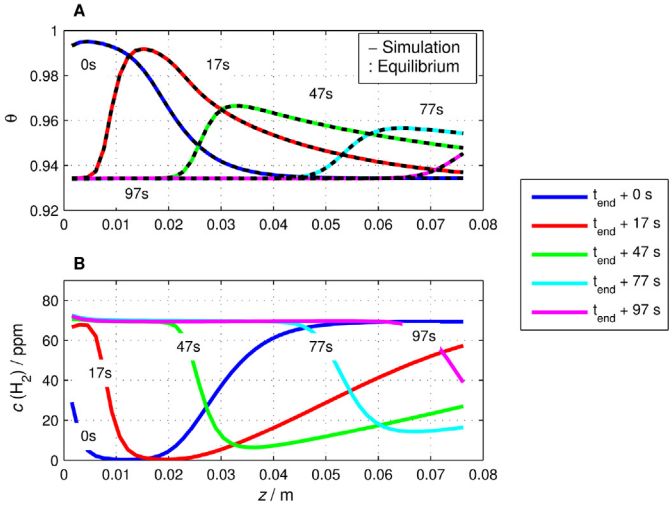


**Fig. 13.** Temporal development of axial concentration profiles after the first oxygen pulse with a duration of 2 s. A) Axial profile of the OSC filling state. The simulated filling level is compared to the filling level at equilibrium (please refer to text). B) Axial concentration profile of $H_2$ in the gas phase.

edge of the oxidized zone, the oxygen storage is oxidized by the reaction with $H_2O$. The combination of reduction by $H_2$ at the front edge and oxidation by $H_2O$ at the rear edge results in the oxidized zone moving downstream towards the outlet of the catalyst. As the zone moves along the catalyst, it broadens and the minimum in the reduction level decreases. When the front edge of the zone hits the outlet, a drop in hydrogen outlet concentration is observed. The delay in the hydrogen signal depends on the time required for the front to reach the outlet. As the length of the oxygen pulse is increased, the length of the initially oxidized zone is also increased and the delay until the front reaches the outlet is reduced. When the oxygen pulse becomes long enough to oxidize the entire catalyst, no delay in the $H_2$ signal is observed anymore.

Fig. 13 also plots the equilibrium filling level computed from the local gas phase concentrations of $H_2$ and $H_2O$ (c.f. Section 3.1). In all cases the filling levels computed by the simulation are virtually identical to the equilibrium values. This implies that the concentration profiles are mainly controlled by the thermodynamics of the oxygen storage reactions and not by the kinetics.

### 3.4.3. *Sensitivity analysis: the impact of thermodynamics on the dynamic catalyst response*

Besides thermodynamics, the response of the catalyst can be controlled by the kinetics of the reactions and by mass transfer effects. To analyze the contribution of the different effects, a sensitivity analysis was performed, where each of the effects was individually varied in the simulation and the impact of this variation on the breakthrough curve was investigated.

*3.4.3.1. Analysis of the $H_2$-response.* In Fig. 14A, the rate of the reduction of $CeO_2$ by $H_2$ (reaction (R1)) has been varied from $0.01\,s^{-1}$ to $100\,s^{-1}$. Note, that a variation in the backward rates automatically induces a corresponding change in the forward rates, since in our model the forward rates are computed from the backward rates and the thermodynamic data presented in Section 3.1. It can be seen that the computed $H_2$ profiles are virtually insensitive to the rate constant and very good agreement with experimental data is obtained, as long as the rate is kept above a threshold of $0.1\,s^{-1}$ (at 500 °C the value used in our model is $5000\,s^{-1}$).

A similar result is obtained for the sensitivity towards the reaction of $CeO_{1.5}$ with $O_2$ (reaction (R3), compare Fig. 14B). Also in this case, the computed $H_2$ profiles are insensitive to the reaction rate, as long as the rate is kept above a threshold of $\sim 10^4\,s^{-1}$ (at 500 °C the value used in the model is $1.2\ 10^4\,s^{-1}$). The sensitivity analysis for the internal and external mass transfer is shown in Figures Fig. 15A and B, respectively. For both effects, the uncertainty in the model parameters is relatively small and as long as the parameters are chosen from a realistic range, the impact of both types of mass transfer limitation is negligible.

Finally, Fig. 15C shows the sensitivity analysis towards the $Ce/ZrO_2$ redox thermodynamics. As expected, already small changes in the thermodynamic parameters have a significant impact on the $H_2$ signal. This is mainly caused by the impact of the thermodynamics on the initial oxygen filling level that determines the available buffer capacity. The sensitivity analysis in Fig. 14 and

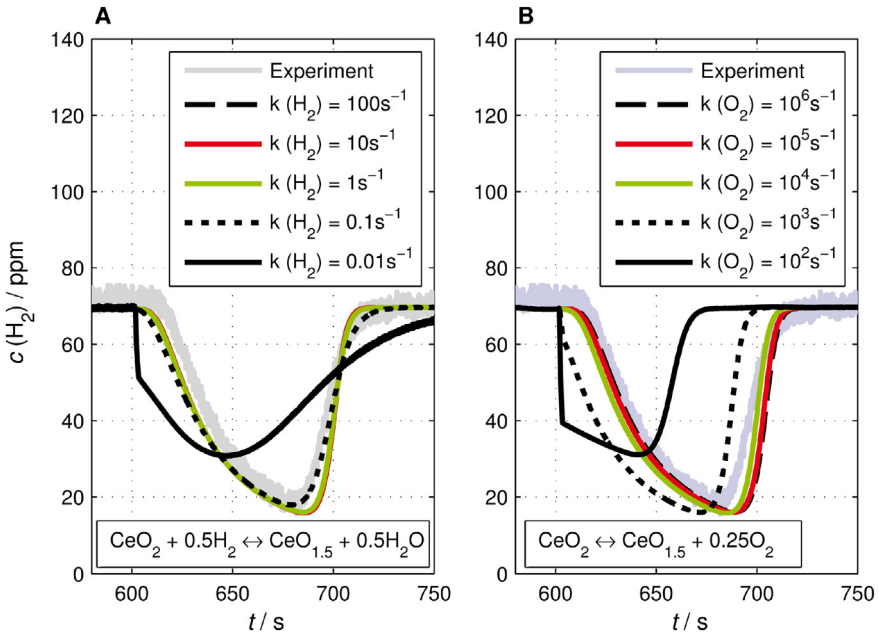


**Fig. 14.** Sensitivity analysis for the $H_2$ response to the first oxygen pulse with a duration of 2 s. A) Variation of the oxygen storage reaction with $H_2/H_2O$. B) Variation of the oxygen storage reaction with $O_2$.

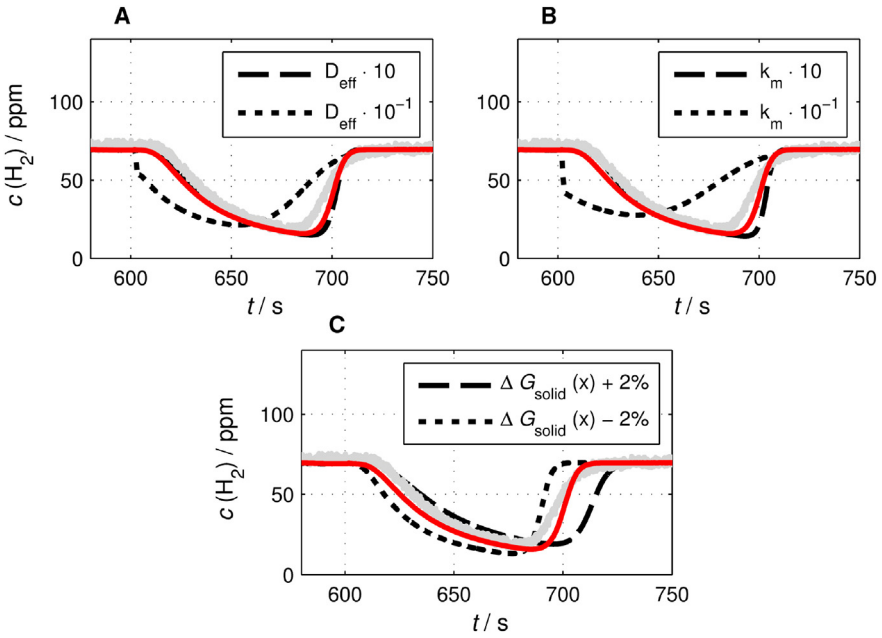


**Fig. 15.** Sensitivity analysis for the $H_2$ response to the first oxygen pulse with a duration of 2 s. A) Variation of the internal diffusion coefficient. B) Variation of the external transfer coefficient. C) Variation of the thermodynamic properties of the oxygen storage.

Fig. 15 was performed at 500 °C. Qualitatively similar results were obtained for the other temperatures (not reported).

In conclusion, the sensitivity analysis shows that the $H_2$ profiles at 500 °C are insensitive to kinetics and mass transfer effects, as long as kinetic and transport parameters are chosen from a realistic range. This means that the transient response of the $H_2$ signals to small $O_2$ pulses is fully determined by the thermodynamics of the oxygen storage with negligible contributions from kinetics and transport effects.

*3.4.3.2. Analysis of the $O_2$-response.* For the oxygen breakthrough, the situation is not as clear as for the $H_2$ response analyzed in the previous section. In the absence of kinetic or mass transfer limitations, one would expect the oxidized zone to move through the catalyst with a sharp rectangular front so that oxygen breakthrough would only be observed after all the oxygen storage was fully oxidized. The amount of oxygen breakthrough would then be equal to the stoichiometric oxygen excess, i.e. the amount of dosed oxygen minus the oxygen required for full oxidation. The stoichiometric oxygen excess is plotted in Fig. 11 by the dashed line. Obviously, in reality oxygen breakthrough is observed slightly earlier than predicted by the dashed line and the difference must be caused by kinetic or mass transfer limitations. To quantify the contribution of the different limiting effects to the early $O_2$ breakthrough, a sensitivity study was performed, which is shown in Fig. 16. Obviously, in contrast to the previously discussed $H_2$ signals, in this case the

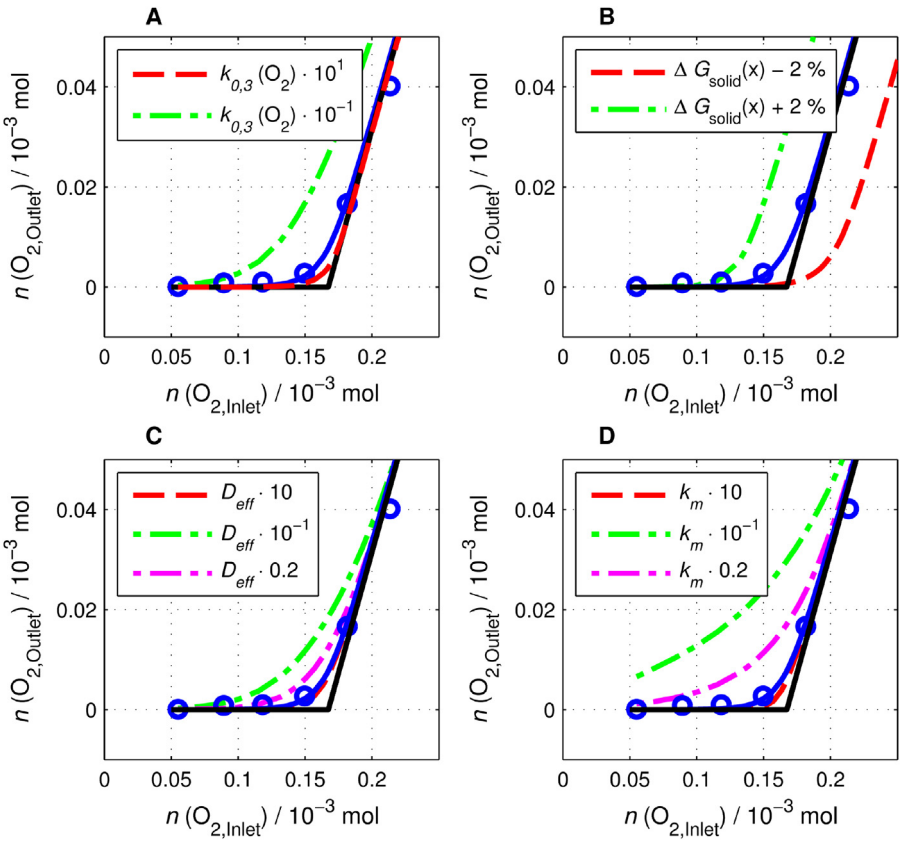


**Fig. 16.** Sensitivity analysis for the $O_2$ response to oxygen pulses. In each study, the experimental data (o, blue) and the reference model (-, blue) as well as the thermodynamic limitation (-, black) are shown. A) Variation of the oxygen storage reaction with $O_2$. B) Variation of the thermodynamic properties of the oxygen storage. C) Variation of the internal diffusion coefficient. D) Variation of the external transfer coefficient. (For interpretation of the references to colour in this figure legend, the reader is referred to the web version of this article.)

kinetics of reaction (R3) as well as internal and external mass transfer all have a significant effect. However, in this case the response is also very sensitive to the thermodynamic data. This is expected, since the thermodynamics determine the oxygen loading of the initial state and hence also the potential oxygen uptake.

## 4. Conclusions

Using a titration scheme, we have measured the redox thermodynamics of the ceria-zirconia oxygen storage in a three-way catalyst. The measurements confirm that under typical vehicle operating conditions the amount of oxygen available from the ceria-zirconia is limited by thermodynamics. Even under very rich conditions (8000 ppm $H_2$/10% $H_2O$) at 500 °C, only about 20% of the stoichiometrically available oxygen can be used. At the typical steady state operating point of a three-way catalyst (lambda sensor voltage of 650 mV, 70 ppm $H_2$, T = 500 °C), the ceria is only reduced to 6%. Our results further suggest that the redox thermodynamics of oxygen storage is not influenced by the precious metal concentration, at least for our measurement conditions and ageing state. Negligible differences were found between the two catalysts with identical oxide composition but different precious metal loadings of 100 g/ft$^3$ and 10 g/ft$^3$.

The importance of thermodynamics has been ignored in much of the discussion of three-way-catalysis in the literature. One important example is the definition of the oxygen storage capacity. The currently accepted definitions of the oxygen storage capacity ignore equilibrium effects and measure the oxygen released during a reduction by $H_2$ or CO in the absence of water. From a thermodynamic point of view, this would lead to the complete reduction of the ceria. In reality, less than complete reduction is obtained, most likely due to kinetic limitations. Our results suggest that measurements under equilibrium controlled conditions (i.e. in the presence of $H_2O$) should lead to a more useful definition of the oxygen storage capacity. First steps in this direction have been published in [35]. It is unclear in how far the oxygen availability under equilibrium constrained conditions correlates with the traditional measurement of oxygen storage capacity. This point is currently addressed in our laboratory.

One further field where equilibrium effects have been ignored in the past is the modeling of three-way catalysts. We have recently presented an equilibrium based oxygen storage model and we have shown that this model explains a number of effects important for lambda control that could not be explained by conventional non-equilibrium models. In our previous model the thermodynamic data was obtained indirectly by simultaneously fitting the kinetic and thermodynamic parameters of a reactor model to experimental data. In the current paper the redox thermodynamics of the same catalyst has been directly measured and a surprisingly good agreement has been found. The good agreement once more underlined the high sensitivity of the transient catalyst response to the thermodynamic data.

To investigate the influence of thermodynamics, mass transfer (in the open channel and in the gas phase) and chemical kinetics on the dynamic response of the catalyst, dynamical oxygen breakthrough experiments have been performed. A kinetic model that uses an equilibrium based oxygen storage model and the thermodynamic data presented in this paper very well reproduces the experimental data. A sensitivity analysis showed that two cases need to be distinguished. For small oxygen pulses that do not lead

to oxygen breakthrough, the downstream response of the $H_2$ signal is nearly completely determined by the redox thermodynamics with very little contribution by kinetics or mass transfer. Accordingly, the catalyst response under these conditions is very well described by the model for a large range of kinetic parameters. For larger oxygen pulses that lead to oxygen breakthrough, the situation is more complicated. In this case, the redox thermodynamics is still important (mainly because it determines the amount of available oxygen), but kinetic and external as well as internal diffusion limitations all play a role.

During typical operation of the lambda control, the oxygen buffer is generally maintained in a partly filled state and oxygen breakthrough is avoided. Our sensitivity analysis shows that under these conditions the response of the catalyst is entirely controlled by the redox equilibrium so that from a control perspective, oxygen storage can be regarded as a thermodynamically controlled process. Consequently, it is important that models used for control design correctly include equilibrium effects and in recent years equilibrium based models have been successfully adopted by the control community [36–39]. The measurement procedure presented in this paper should provide an accurate data basis for such model based control design applications. Furthermore, the direct measurement of the redox thermodynamics in the future should help to link structure, composition and synthesis conditions of the ceria mixed oxides to the redox properties. Ultimately, this should lead to a more rational development of oxygen storage materials, especially with respect to an improved interaction with the lambda control.

## Acknowledgements

The authors thank Prof. Herbert Vogel and Dr. Alfons Drochner from the TU Darmstadt for helpful discussions on the subject of this paper. This work was supported by the Bundesministerium für Bildung und Forschung (project REFFKAT, grant number 03X3563A).

## Appendix A. Supplementary data

Supplementary data associated with this article can be found, in the online version, at http://dx.doi.org/10.1016/j.apcatb.2016.12.052.

## References

[1] R.J. Gorte, Ceria in catalysis: from automotive applications to the water-gas shift reaction, AIChE J. 56 (5) (2010) 1126–1135.
[2] M. Sugiura, Oxygen storage materials for automotive catalysts: ceria-zirconia solid solutions, Catal. Surv. Asia 7 (1) (2003) 77–87.
[3] J. Wang, H. Chen, Z. Hu, M. Yao, Y. Li, A review on the Pd-based three-way catalyst, Catal. Rev. 57 (1) (2015) 79–144.
[4] R. Möller, M. Votsmeier, C. Onder, L. Guzzella, J. Gieshoff, Is oxygen storage in three-way catalysts an equilibrium controlled process? Appl. Catal. B: Environ. 91 (1–2) (2009) 30–38.
[5] D. Bevan, J. Kordis, Mixed oxides of the type $MO_2$ (fluorite)–$M_2O_3$–I. Oxygen dissociation pressures and phase relationships in the system $CeO_2$—$Ce_2O_3$ at high temperatures, J. Inorg. Nucl. Chem. 26 (9) (1964) 1509–1523.
[6] M. Eufinger, K. Daniels, S. Schmale, G. Berendts, M. Ulbrich, H.-D. Wiemhofer, J. Janek, The model case of an oxygen storage catalyst – non-stoichiometry, point defects and electrical conductivity of single crystalline $CeO_2$-$ZrO_2$-$Y_2O_3$ solid solutions, Phys. Chem. Chem. Phys 16 (2014) 25583–25600.
[7] R. Gorte, S. Zhao, Studies of the water-gas-shift reaction with ceria-supported precious metals, Catal. Today 104 (1) (2005) 18–24.
[8] R. Panlener, R. Blumenthal, J. Garnier, A thermodynamic study of nonstoichiometric cerium dioxide, J. Phys. Chem. Solids 36 (11) (1975) 1213–1222.
[9] A. Trovarelli, P. Fornasiero, Catalysis by Ceria and Related Materials, second ed., Imperial College Press, London, 2013.
[10] H. Otobe, A. Nakamura, T. Yamashita, K. Minato, Oxygen potential and defect structure of oxygen-excess pyrochlore $Ce_2Zr_2O_{7+x}$, J. Phys. Chem. Solids 66 (2–4) (2005) 329–334.
[11] T. Kim, J.M. Vohs, R.J. Gorte, Thermodynamic investigation of the redox properties of ceria-zirconia solid solutions, Ind. Eng. Chem. Res. 45 (16) (2006) 5561–5565.
[12] P.R. Shah, T. Kim, G. Zhou, P. Fornasiero, R.J. Gorte, Evidence for entropy effects in the reduction of ceria-zirconia solutions, Chem. Mater. 18 (22) (2006) 5363–5369.
[13] G. Zhou, P.R. Shah, T. Montini, P. Fornasiero, R.J. Gorte, Oxidation enthalpies for reduction of ceria surfaces, Surf. Sci. 601 (12) (2007) 2512–2519.
[14] H.-F. Wang, Y.-L. Guo, G.-Z. Lu, P. Hu, Maximizing the localized relaxation: the origin of the outstanding oxygen storage capacity of κ-$Ce_2Zr_2O_8$, Angew. Chem. Int. Ed. 48 (44) (2009) 8289–8292.
[15] M. Kuhn, S. Bishop, J. Rupp, H. Tuller, Structural characterization and oxygen nonstoichiometry of ceria-zirconia ($Ce_{1-x}Zr_xO_{2-\delta}$) solid solutions, Acta Mater. 61 (11) (2013) 4277–4288.
[16] Y. Hao, C.-K. Yang, S.M. Haile, Ceria-zirconia solid solutions ($Ce_{1-x}Zr_xO_{2-\delta}$, $x < 0.2$) for solar thermochemical water splitting: a thermodynamic study, Chem. Mater. 26 (20) (2014) 6073–6082.
[17] S. Bernal, G. Blanco, J. Calvino, J. Gatica, J. Omil, J. Pintado, Characterisation of three-way automotive aftertreatment catalysts and related model systems, Top. Catal. 28 (2004) 31–45.
[18] C. Descorme, R. Taha, N. Mouaddib-Moral, D. Duprez, Oxygen storage capacity measurements of three-way catalysts under transient conditions, Appl. Catal. A: Gen. 223 (1–2) (2002) 287–299.
[19] N. Hickey, P. Fornasiero, J. Kašpar, M. Graziani, G. Blanco, S. Bernal, Significant room temperature oxygen storage over 0.58% $Pt/Ce_{0.68}Zr_{0.32}O_2$ when $H_2$ is used as a reducing agent, Chem. Commun. (2000) 357–358.
[20] N. Hickey, P. Fornasiero, R. DiMonte, J. Kašpar, M. Graziani, G. Dolcetti, A comparative study of oxygen storage capacity over $Ce_{0.6}Zr_{0.4}O_2$ mixed oxides investigated by temperature-programmed reduction and dynamic OSC measurements, Catal. Lett. 72 (1) (2001) 45–50.
[21] H. Yao, Y. Yao, Ceria in automotive exhaust catalysts: i. oxygen storage, J. Catal. 86 (2) (1984) 254–265.
[22] A. Trovarelli, Catalytic properties of ceria and $CeO_2$-containing materials, Catal. Rev. 38 (4) (1996) 439–520.
[23] M. Boaro, F. Giordano, S. Recchia, V.D. Santo, M. Giona, A. Trovarelli, On the mechanism of fast oxygen storage and release in ceria-zirconia model catalysts, Appl. Catal. B Environ. 52 (3) (2004) 225–237.
[24] J. Kašpar, On the role of oxygen storage in three-way catalysis, Top. Catal. 28 (1–4) (2004) 47–57.
[25] Y. Sakamoto, K. Kizaki, T. Motohiro, Y. Yokota, H. Sobukawa, M. Uenishi, H. Tanaka, M. Sugiura, New method of measuring the amount of oxygen storage/release on millisecond time scale on planar catalyst, J. Catal. 211 (1) (2002) 157–164.
[26] G.C. Koltsakis, A.M. Stamatelos, Modeling dynamic phenomena in 3-way catalytic converters, Chem. Eng. Sci. 54 (20) (1999) 4567–4578.
[27] K. Bakhmutsky, G. Zhou, S. Timothy, R. Gorte, The water-gas-shift reaction on Pd/ceria-praseodymia: the effect of redox thermodynamics, Catal. Lett. 129 (1–2) (2009) 61–65.
[28] T. Bunluesin, R. Gorte, G. Graham, Studies of the water-gas-shift reaction on ceria-supported Pt, Pd, and Rh: implications for oxygen-storage properties, Appl. Catal. B: Environ. 15 (1–2) (1998) 107–114.
[29] C. Padeste, N. Cant, D. Trimm, The influence of water on the reduction and reoxidation of ceria, Catal. Lett. 18 (3) (1993) 305–316.
[30] S. Sharma, S. Hilaire, J. Vohs, R. Gorte, H.-W. Jen, Evidence for oxidation of ceria by $CO_2$, J. Catal. 190 (1) (2000) 199–204.
[31] The total precious metal loading war erroneously reported as 10 g/ft3 in our previous communication [4]. We apologize for the mistake.
[32] R. Möller, C. Onder, L. Guzzella, M. Votsmeier, J. Gieshoff, Analysis of a kinetic model describing the dynamic operation of a three-way catalyst, Appl. Catal. B: Environ. 70 (1–4) (2007) 269–275.
[33] E. Tronconi, P. Forzatti, Adequacy of lumped parameter models for SCR reactors with monolith structure, AIChE J. 38 (2) (1992) 201–210.
[34] C. Morley, http://www.arcl02.dsl.pipex.com.
[35] G. Keitl, J. Rink, F. Wen, L. Jongen, A. Hofmann, M. Votsmeier, A. Terfort, J. Gieshoff, Impact of test conditions on the oxygen storage capacity of Pd loaded cerium zirconium oxide, Top. Catal. (2016) 1–6.
[36] N. Bekiaris-Liberis, M. Jankovic, M. Krstic, PDE-based analysis and control of the oxygen storage level in three-way catalytic converters, 51st IEEE Conf. Decis. Control (CDC) (2012) 3759–3764.
[37] S. Schödel, R. Moos, M. Votsmeier, G. Fischerauer, SI-engine control with microwave-assisted direct observation of oxygen storage level in three-way catalysts, IEEE Trans. Control Syst. Technol. 22 (6) (2014) 2346–2353.
[38] M. Santillo, S. Magner, M. Uhrich, M. Jankovic, Towards ECU-executable control-oriented models of a three-way catalytic converter, ASME P 3 (2015) (2015) 1–9.
[39] R. Stanchev, U. Konigorski, M. Votsmeier, Modellbildung und Vergleich von linearen und nichtlinearen Regelungskonzepten für Drei-Wege-Abgaskatalysatoren, Automatisierungstechnik 64 (4) (2016) 297–311.